ISSN 0036-0295, Russian Metallurgy (Metally), Vol. 2014, No. 9, pp. 721–724. © Pleiades Publishing, Ltd., 2014.
Original Russian Text © E.N. Kablov, V.P. Piskorskii, R.A. Valeev, O.G. Ospennikova, I.I. Rezchikova, N.V. Volkov, K.A. Shaikhutdinov, 2014, published in Metally, 2014, No. 5, pp. 47–51.

Boron Mobility in Sintered (Pr, Dy)–(Fe, Co)–B Materials with a High Cobalt Content

E. N. Kablov[a], V. P. Piskorskii[a], R. A. Valeev[a], O. G. Ospennikova[a], I. I. Rezchikova[a], N. V. Volkov[b], and K. A. Shaikhutdinov[b]

[a] *All-Russia Research Institute of Aviation Materials, ul. Radio 17, Moscow, 105005 Russia*
e-mail: vppvpp@rambler.ru
[b] *Kirenskii Institute of Physics, Siberian Branch, Russian Academy of Sciences, ul. Akademgorodok 50, build. 38, Krasnoyarsk, 660036 Russia*
e-mail: volk@iph.krasn.ru

Received February 6, 2014

Abstract—Sintered (Pr, Dy)–$(Fe_{1-y}Co_y)$–B materials with up to $y \approx 0.5$ atomic fractions have been studied. Boron is found to be a movable element, and its diffusion between principal magnetic phase A and other boron-containing phases determines the properties of the materials. The structure of principal magnetic phase grains is sufficiently complex: their periphery is enriched in boron. The enrichment is shown to cause a decrease in the coercive force of the materials to zero after sintering.

DOI: 10.1134/S0036029514090080

INTRODUCTION

Sintered (Pr, Dy)–(Fe, Co)–B compositions with a high cobalt content are, first of all, materials for inertial navigation instruments [1, 2]. The main requirement for the hard magnetic materials applied in such instruments consists in temperature-independent saturation magnetization J_s along with maximum coercive force H_{cJ} and remanent induction B_r [3]. To obtain these characteristics, all rare-earth metal-based magnets should be alloyed with heavy rare-earth metals (REMs), and Nd–Fe–B-based compositions should also be alloyed with cobalt [4, 5]. Alloying with both cobalt and heavy REMs leads to a decrease in J_s and B_r; the decrease in the both parameters is more substantial when the materials are alloyed with heavy REMs, since their magnetic moments and those of the 3*d* sublattice of the magnetic material are arranged antiferromagnetically. Therefore, alloying with cobalt is more preferable. However, it was found in [6] that, as the cobalt content in sintered (Pr, Dy)–$(Fe_{1-y}Co_y)$–B materials increases to $y \approx 0.5$ atomic fractions, coercive force H_{cJ} decreases to almost zero. This study is related to an investigation of sintered (Pr, Dy)–$(Fe_{1-y}Co_y)$–B materials with cobalt contents $y \geq 0.35$ atomic fractions.

EXPERIMENTAL

The compositions of sintered materials are given in the table. The preparation technology of sintered magnets is described in [5, 6]. The magnetic characteristics were measured in the temperature range from –60 to +80°C using a PPMS-9 instrument and spherical samples. The samples were magnetized in a field of

Compositions of samples and their magnetic characteristics including TCI measured in the temperature range from –60 to + 80°C in applied magnetic fields of 1600 and 320 kA/m

Material*	B_r, T	$4\pi J_s$, T	H_{cJ}, kA/m	TCI, %/°C measured in magnetic field H, kA/m	
				1600	320
$(Pr_{0.52}Dy_{0.48})_{13.6}(Fe_{0.65}Co_{0.35})_{bal}B_{6.9}$	0.83	0.91	1240	–	–
$(Pr_{0.73}Dy_{0.26})_{13.7}(Fe_{0.51}Co_{0.49})_{bal}B_{8.4}$	0.92	1.06	400	–0.036	–0.034
$(Pr_{0.49}Dy_{0.31})_{16.1}(Fe_{0.47}Co_{0.53})_{bal}B_{16.7}$	0.53	0.74	800	–0.061	–0.051
$(Pr_{0.49}Dy_{0.51})_{14.4}(Fe_{0.56}Co_{0.44})_{bal}B_{6.5}$	0.77	0.84	400	+0.068	+0.015

* The material composition is given in at %.

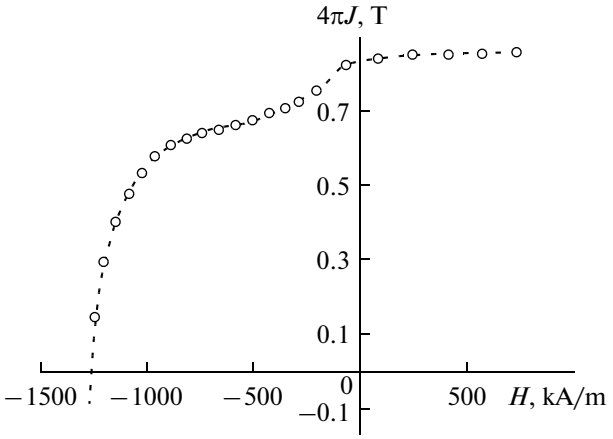

Fig. 1. Demagnetization curve for the sintered $(Pr_{0.52}Dy_{0.48})_{13.6}(Fe_{0.65}Co_{0.35})_{bal}B_{6.9}$ material at 20°C.

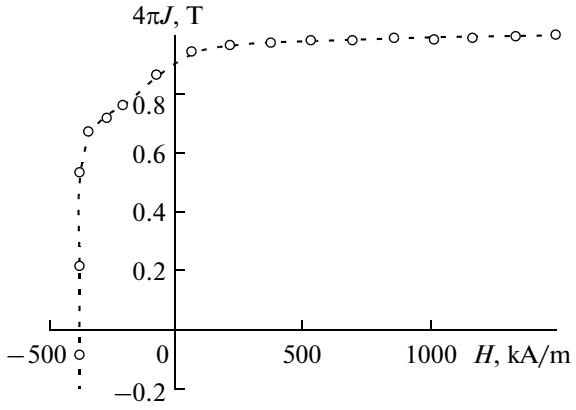

Fig. 2. Demagnetization curve for the sintered $(Pr_{0.73}Dy_{0.26})_{13.7}(Fe_{0.51}Co_{0.49})_{bal}B_{8.4}$ material at 20°C.

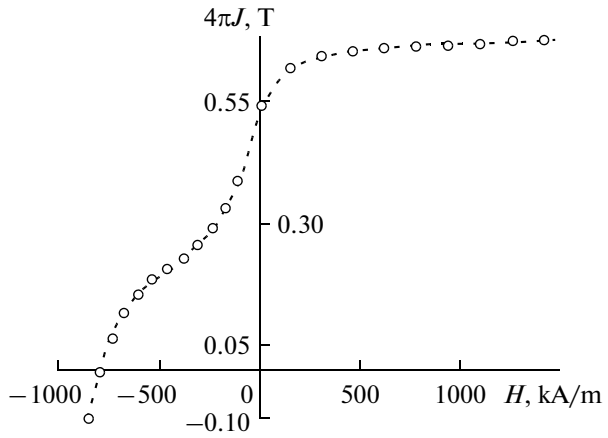

Fig. 3. Demagnetization curve for the sintered $(Pr_{0.69}Dy_{0.31})_{16.1}(Fe_{0.47}Co_{0.53})_{bal}B_{16.7}$ material at 20°C.

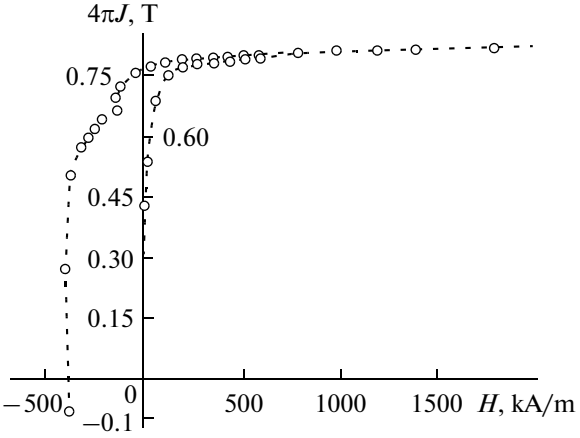

Fig. 4. Magnetic hysteresis curve for the sintered $(Pr_{0.49}Dy_{0.51})_{14.4}(Fe_{0.56}Co_{0.44})_{bal}B_{6.5}$ material at 20°C.

7200 kA/m. During measurements, the magnetic texture of the samples was parallel to an applied magnetic field.

RESULTS

Figures 1–4 show the magnetization curves of the materials at 20°C (see table). Figure 5 shows the temperature dependences of the saturation magnetization of two samples measured in applied magnetic fields of 1600 and 320 kA/m. According to these data (see Figs. 1–4 and table), H_{cJ} decreases abruptly with increasing cobalt content in the sintered materials. It was noted in [5–7] that the cause for the decrease consists in an increase in the fraction of boron-containing phases. It is seen from Figs. 2 and 3 that, at a cobalt content of about 0.5 atomic fractions in the material, an increase in the boron content leads to an abrupt increase in H_{cJ} from 400 to 800 kA/m, but the squareness ratio of hysteresis loop worsens. As is seen from the table (second and third lines), an increase in the boron content from 8.4 to 16.7 at % leads to an abrupt (30%) decrease in the saturation magnetization at room temperature, a cobalt content of ~0.5 atomic fractions, and almost equal dysprosium contents. It is also seen from the data given in the table that, in this case, the temperature coefficient of induction (TCI) increases by 69%, although the effect should be inverse since the amounts of cobalt and dysprosium increase though slightly [5–7]. An analysis of the magnetization curve of the $(Pr_{0.49}Dy_{0.51})_{14.4}(Fe_{0.56}Co_{0.44})_{bal}B_{6.5}$ material (Fig. 4) shows that, in a field of 800 kA/m, the sample is magnetized to saturation. A maximum in the temperature dependence of J_s measured in the temperature range from –60 to +80°C is observed only for the $(Pr_{0.52}Dy_{0.48})_{13.6}(Fe_{0.65}Co_{0.35})_{bal}B_{6.9}$ sample (Fig. 5a). The temperature of the maximum (T_{max}) is ~30°C and is independent on the applied magnetic field. As follows from the value of TCI (see table), the temperature dependence of the saturation magnetization mea-

sured for the $(Pr_{0.49}Dy_{0.51})_{14.4}(Fe_{0.56}Co_{0.44})_{bal}B_{6.5}$ sample in the temperature range from –60 to +80°C should also have a maximum at $T_{max} > 80$°C.

DISCUSSION OF RESULTS

The behavior of the magnetization reversal curve given in Fig. 2 differs substantially from that shown in Fig. 3. The abrupt decrease in $4\pi J$ in low magnetic fields (~100 kA/m) (Fig. 3) means that magnetization reversal starts in these fields. Reverse magnetization domains nucleate in the areas characterized by a lower anisotropy constant [8]. This is the cause of the difference in the magnetization reversal curves given in Figs. 2 and 3. The substitution of boron atoms for iron and cobalt ions in the $(Pr_{0.73}Dy_{0.26})_{13.7}(Fe_{0.51}Co_{0.49})_{bal}B_{8.4}$ magnetic material takes place only in the surface areas of principal $R_2(Fe, Co)_{14}B$ magnetic phase (phase A) grains (thereinafter, R = REM). The replacement of iron and cobalt ions with boron atoms is likely to occur during sintering; the probability of almost complete substitution of boron ions for iron and cobalt ions at least in the nearest environment of R ion is high. This leads to the disappearance of exchange coupling between the magnetic moments of the R and F (F = Fe + Co) sublattices and, therefore, to a low coercive force ($H_{cJ} = 800$ kA/m).

The degree of substitution of boron ions for iron and cobalt ions within the internal areas of A-phase grains of the $(Pr_{0.69}Dy_{0.31})_{16.1}(Fe_{0.47}Co_{0.53})_{bal}B_{16.7}$ sintered material is rather low. In this case, no decoupling between the R and F sublattices takes place: only $4\pi J_s$ decreases, since it is mainly determined by the F sublattice [9]. As a result, the shape of the demagnetization curve is far from squareness (see Fig. 3). Such a shape of the demagnetization curve results from the complex structure of A-phase grains: at the periphery of the grains, boron ions substitute for many iron and cobalt ions, and the exchange interaction between the R and F sublattices is disturbed. This results in a decrease in anisotropy field H_a of the outer area of A-phase grains.

Thus, the area close to the surface of A-phase grains is responsible for the abrupt decrease in the magnetization in low fields, whereas the core area of A-phase grains is responsible for the magnitude H_{cJ} = 800 kA/m. The anisotropy field of the $R_2Fe_{14}B$ compound with R = Pr and Dy at room temperature is 6960 and 12000 kA/m, respectively [9]. That is why the behavior of the temperature dependence of magnetization is unchanged when $4\pi J$ is measured in applied fields of 1600 and 320 kA/m (see Fig. 5a). In other words, the "height" of the maximum in the temperature dependence of magnetization and its position are independent of the field applied during measurements. Therefore, we can conclude that the inspection of sintered materials used in instruments for inertial navigation can be performed with a vibrating-sample magnetometer, since the magnetic field applied during measurements is much lower than the aforementioned anisotropy fields of the A phase in the materials.

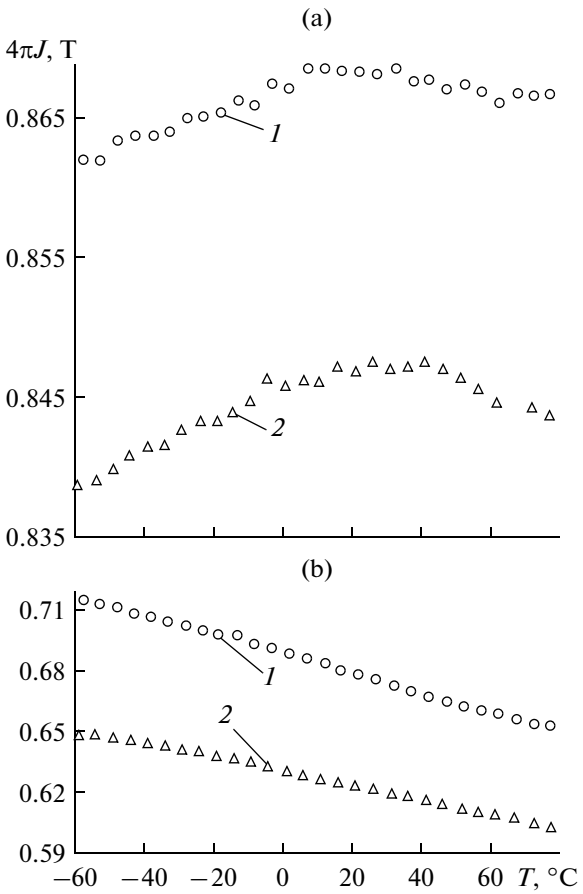

Fig. 5. Temperature dependences of the magnetization of the sintered materials (a) $(Pr_{0.52}Dy_{0.48})_{13.6}(Fe_{0.65}Co_{0.35})_{bal}B_{6.9}$ and (b) $(Pr_{0.69}Dy_{0.31})_{16.1}(Fe_{0.47}Co_{0.53})_{bal}B_{16.7}$ that were measured in magnetic fields of (*1*) 1600 and (*2*) 320 kA/m on spherical samples. A magnetic field was applied parallel to the sample texture.

The shape of the magnetization curve (Fig. 4) allows us to conclude that the magnetic hardness formation mechanism in the materials is determined by the nucleation of magnetization reversal centers rather than the pinning of domain walls by barriers [9]. TCI for the sintered $(Pr_{0.69}Dy_{0.31})_{16.1}(Fe_{0.47}Co_{0.53})_{bal}B_{16.7}$ materials in the temperature range from –60 to +80 is –0.061 and –0.051%/°C in fields of 1600 and 320 kA/m, respectively (see table). The sufficiently high value of TCI indicates that, in spite of a significant cobalt content in the material, a dysprosium content of 0.31 atomic fractions in the material is insufficient to obtain near-zero TCI at temperatures from –60 to +80°C. In other words, to use the sintered materials in navigation instruments, alloying with heavy REMs is necessary along with an increase in the cobalt content (i.e., increase in the Curie temperature).

CONCLUSIONS

(1) The shape of the temperature dependence of the magnetization of sintered (Pr, Dy)–$(Fe_{1-y}Co_y)$–B materials with $y \geq 0.35$ atomic fractions is independent of the magnetic field applied during measurements.

(2) The magnetic hardness formation mechanism in the (Pr, Dy)–$(Fe_{1-y}Co_y)$–B materials with $y \geq 0.35$ atomic fractions is determined by the nucleation of magnetization reversal centers rather than by the pinning of domain walls by barriers.

(3) The vanishing of the coercive force H_{cJ} of sintered (Pr, Dy)–$(Fe_{1-y}Co_y)$–B materials with $y \approx 0.5$ atomic fractions is caused by boron diffusion from boron-containing phases into the principal magnetic phase during sintering.

(4) The grains of the principal $(Pr, Dy)_2(Fe, Co)_{14}B$ magnetic phase in the sintered (Pr, Dy)–$(Fe_{1-y}Co_y)$–B materials with $y \approx 0.5$ atomic fractions are characterized by areas differing in the boron content. When boron ions substitute for iron and cobalt ions in the outer area of magnetic-phase grains, the exchange coupling of the REM, on the one hand, and Fe and Co sublattices is broken, which results in an abrupt decrease of H_{cJ} of sintered materials. An increase in the boron content in the sintered materials leads to an increase in the boron-enriched outer area of grains; in this case, the coercive force increases and the squareness ratio of the magnetization curve degrades.

REFERENCES

1. *Aviation Materials and Technologies*, Ed. by E. N. Kablov (VIAM, Moscow, 2012).
2. E. N. Kablov, "Strategic directions in developing materials and their processing technologies up to 2030", in *Aviation Materials and Technologies: Jubilee Scientific and Technical Collection, Supplement* (VIAM, Moscow, 2012), pp. 7–17.
3. V. Ya. Raspopov, *Micromechanical Instruments* (Mashinostroenie, Moscow, 2007).
4. W. Suski, R. Gladyshevskii, A. Gilewski, T. Mydlarz, and K. Wochowski, "Magnetic properties of $Ln_{2.1}Co_{16.9}Si$ alloys," Chem. Met. Alloys, No. 1, 34–37 (2008).
5. E. N. Kablov, A. F. Petrakov, V. P. Piskorskii, R. A. Valeev, and N. V. Nazarova, "Effect of dysprosium and cobalt on the temperature dependence of the magnetization and phase composition of a material of the Nd–Dy–Fe–Co–B system," Metalloved. Term. Obrab. Met., No. 4, 3–10 (2007).
6. V. P. Piskorskii, R. A. Valeev, A. V. Buzenkov, E. A. Davydova, and M. V. Zolotareva, "Effect of high cobalt contents on the properties of Pr–Dy–Fe–Co–B magnets," Perspektivnye Materialy, Special Issue, March, 268–271 (2008).
7. E. N. Kablov, V. P. Piskorskii, R. A. Valeev, O. G. Ospennikova, and I. I. Rezchikov, "Role of boron in the formation of the magnetic properties of sintered Nd–Dy–Fe–Co–B materials with a high cobalt content," Russian Metallurgy (Metally), No. 3, 202–203 (2014).
8. J. Fidler, T. Schrefl, S. Sasaki, and D. Suess, "The role of intergranular regions in sintered Nd–Fe–B magnets with $(BH)_{max} > 420$ kJ/m^3 (52.5 MGOe)," in *Proceedings of XI International Symposium on Magnetic Anisotropy and Coercivity in Rare Earth Transition Metal Alloys*, Ed. by H. Kaneko, M. Homma, M. Okada, (The Jpn. Inst. Met., Sendai, 2000), pp. S45–S54.
9. K. H. J. Buschow, "New development in hard magnetic materials," Rep. Prog. Phys. **54** (9), 1125–1214 (1991).

Translated by N. Kolchugina